

PL and TL behaviors of Ag-doped SnO₂ nanoparticles: effects of thermal annealing and Ag concentration

R. Sánchez Zeferino^{1a}, U. Pal^{*1}, R. Meléndrez^{2b} and M. Barboza Flores^{2c}

¹Instituto de Física, Universidad Autónoma de Puebla, Apdo. Postal J-48, Puebla, Pue. 72570, Mexico

²Centro de Investigación en Física, Universidad de Sonora, Apartado Postal 5-088, Hermosillo, Sonora 83190, Mexico

(Received June 21, 2012, Revised October 22, 2013, Accepted October 23, 2013)

Abstract. In this article, we present the effects of Ag doping and after-growth thermal annealing on the photoluminescence (PL) and thermoluminescence (TL) behaviors of SnO₂ nanoparticles. SnO₂ nanoparticles of 4-7 nm size range containing different Ag contents were synthesized by hydrothermal process. It has been observed that the after-growth thermal annealing process enhances the crystallite size and stabilizes the TL emissions of SnO₂ nanostructures. Incorporated Ag probably occupies the interstitial sites of the SnO₂ lattice, affecting drastically their emission behaviors on thermal annealing. Both the TL response and dose-linearity of the SnO₂ nanoparticles improve on 1.0% Ag doping, and subsequent thermal annealing. However, a higher Ag content causes the formation of Ag clusters, reducing both the TL and PL responses of the nanoparticles.

Keywords: tin oxide; nanoparticle; Ag-doping; photoluminescence; thermoluminescence

1. Introduction

Synthesis of quantum confined tin oxide (SnO₂) nanoparticles has been a subject of intense research in recent years due to strong carrier confinement (Lee *et al.* 2004), high surface-to-volume ratio (Baik *et al.* 2000) and enhanced surface modes in their Raman spectra (Zuo *et al.* 1994), which are some interesting features of metal oxide nanoparticles for their applications in gas sensing, catalysis, and optoelectronics such as light emitting diode (Epifani *et al.* 2008, Qian *et al.* 2007, Yang *et al.* 2010). Though a considerable effort has been given to obtain stoichiometric low-dimensional SnO₂ structures of different morphologies to keep their optoelectronic properties unaltered (unchanged surface states), applied synthesis procedures have seen to affect substantially the microstructure, crystallinity and defect structure of the nanostructures. Several methods including hydrothermal (Chen *et al.* 2009), sol-gel (Gnanam and Rajendran 2010), electrospinning (Qia *et al.* 2009) have been utilized to synthesize SnO₂ nanostructures at relatively low

*Corresponding author, Professor, E-mail: upal@sirio.ifuap.buap.mx

^aResearch Scholar, E-mail: raulsz@ifuap.buap.mx

^bProfessor, E-mail: rodrigo@cajeme.cifus.uson.mx

^cProfessor, E-mail: mbarboza@cajeme.cifus.uson.mx

temperatures (80-200°C) which can lead to a relaxation in the interface structure, none of them seems to dispel the local lattice disorder (i.e., hydroxyl groups, oxygen vacancies) or change in the internal grain structures (Yu *et al.* 1997). Since most of the nanomaterials constitute grain structures, any change in their internal microstructure can straightway modify their physical and chemical properties. Frequently a post synthesis thermal treatment is used to improve the crystallinity of SnO₂ nanostructures, which also improves their thermoluminescence (TL) response as has been demonstrated for LiF:Mg phosphors by Lee *et al.* (2011).

In this article, the effects of after-growth thermal treatments on the optical and emission behaviors of undoped and Ag-doped SnO₂ nanoparticles have been studied. The nanoparticles were synthesized by hydrothermal technique with different Ag contents, and annealed at different temperatures (300 and 700°C) in air. Effects of Ag content on the photoluminescence (PL) and thermoluminescence (TL) behaviors of the nanoparticles have been discussed.

2. Experimental

Tin oxide nanoparticles were prepared using hydrothermal method at relatively low temperature (Pal *et al.* 2012). A typical synthesis process started with the preparation of two aqueous solutions by dissolving 5.25 g, and 3.0 g of tin (IV) chloride pentahydrate (SnCl₄•5H₂O, Sigma-Aldrich, 98 %) and sodium hydroxide (NaOH, J.T. Baker, 98.15 %) in 10.0 mL and 30.0 mL of deionized water, respectively. The NaOH solution was then drop-wise added to the tin chloride solution under magnetic agitation until the pH of the mixture solution reaches close to 7.0. Then 45.0 mL of absolute anhydrous ethanol (C₂H₅OH, J. T. Baker, 99.8 %) was added to the mixture. The final pH of the mixture was adjusted to 7.0 by adding the required amount of the NaOH solution. For preparing Ag-doped SnO₂ samples, silver nitrate (AgNO₃, Sigma-Aldrich, 99 %) was added to the reaction mixture under vigorous stirring before adjusting their final pH to 7.0. AgNO₃ contents in the solution were adjusted to maintain nominal concentration of Ag either 1.0 or 5.0 mol %. Thereafter, the mixture solution was transferred into a Teflon-lined stainless-steel autoclave and treated hydrothermally at 190°C for 24 h. After passively cooling the autoclave to room temperature, the precipitate formed at the bottom was separated by centrifuging at 8000 rpm for 20 min, washed several times by addition of ethanol, and dried in a muffle furnace at 65°C for 2 h. Finally, the obtained powder samples were annealed either at 300°C or 700°C for 2 h in air.

Crystallinity and structural phase of the samples were verified through powder X-ray diffraction (XRD) and transmission electron microscopy (TEM) techniques. For XRD traces, the Cu K α ($\lambda=1.5406\text{\AA}$) emission of a Bruker D8 Discover diffractometer was utilized. A JEOL FEG 2010F FasTem electron microscope operating at 200 keV was used to obtain the images of the samples. For TEM observations, the powder samples were dispersed in ethanol under ultrasonic agitation and dispersed over carbon-coated copper microgrids. Optical properties of the nanoparticles were studied by micro-Raman spectroscopy (Horiba JOBIN-YVON spectrophotometer), and photoluminescence (PL) spectroscopy at room temperature. While the 634 nm line of a He-Ne laser source (5 mW) was utilized for micro-Raman measurements, the 325 emission line of a He-Cd laser source (Melles Griot, 10 mW) was utilized for exciting the samples during PL measurements. TL measurements on the samples were performed in a Risø TL/OSL model TL/OSL-DA-15 unit equipped with a ⁹⁰Sr beta source. The TL measurements were carried out under N₂ atmosphere using a heating rate of 5°C/s.

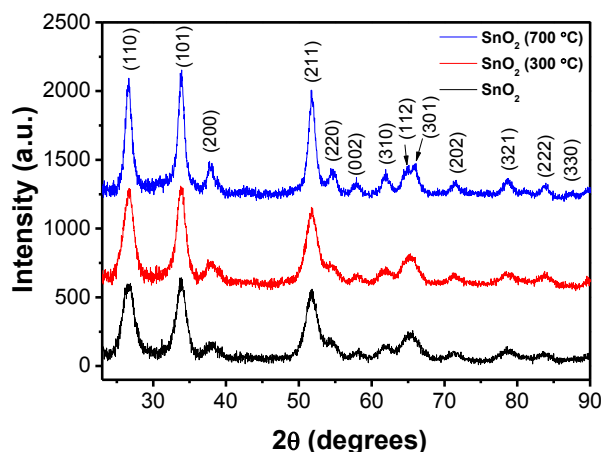


Fig. 1 XRD patterns of the undoped SnO₂ nanoparticles annealed at different temperatures for 2 h, in air

3. Results and discussion

Fig. 1 shows the XRD patterns of the undoped SnO₂ nanoparticles air-annealed at different temperatures. XRD peaks of all the samples correspond well with the tetragonal rutile phase of SnO₂ (JCPDS file no. 77-0451). With the increase of annealing temperature, the diffraction peaks sharpened and their intensity enhanced; indicating an increase in particle size, and improvement of crystallinity. As can be seen, all the samples revealed broad XRD peaks (wide full-width at half maximum, FWHM) due to their small particle size. XRD patterns of the as-grown and annealed Ag-doped SnO₂ samples are presented in Fig. 2. The Ag-doped samples also revealed their tetragonal crystalline phase. However, on thermal annealing at 700°C the intensity of their XRD peaks increased drastically.

In order to determine the average crystallite size (*D*) of the undoped and Ag-doped SnO₂ samples from their XRD patterns, we used the Scherrer formula:

$$D = \frac{0.9\lambda}{\beta \cos \theta}$$

where β is the FWHM, θ is the Bragg angle, and λ is the X-rays wavelength.

From Table 1, we can easily notice the increase of crystallite size of the undoped SnO₂ sample on air-annealing. On thermal annealing at 700°C, the crystallite size increased from 6.0 to 11.3 nm and from 5.0 to 10.0 nm for the 1.0 % and 5.0 % Ag doped sample, respectively. The increase of crystallite size in the annealed samples is the result of thermal diffusion-induced growth of crystalline grains. Such diffusion induced bonding of smaller grains (to form bigger grains) basically reduces the surface energy of the powder samples by reducing free surfaces, along with the reduction of grain boundary area via grain growth (German 1996). The diffusion-induced bonding of small grains (to form bigger crystalline grains) is clear from the TEM micrographs of the annealed and unannealed SnO₂ samples presented in Fig. 3.

Tetragonal rutile phase SnO₂ crystallizes in the D_{4h}^{14} space group containing two metal atoms and four oxygen atoms in its unit cell. According to the group theory, SnO₂ crystals should have 15 lattice vibration modes:

$$\Gamma_{rutile} = A_{1g} + A_{2g} + A_{2u} + B_{1g} + B_{2g} + 2B_u + E_g + 3E_u$$

where A_{1g} , B_{1g} , B_{2g} (non-degenerate modes) and E_g (the doubly degenerate) are Raman active, A_{2u} and E_u (the triply degenerate) are IR active acoustic modes and A_{2g} and B_u are silent modes (Yu *et al.* 1997).

Fig. 4 shows the Raman spectra of the undoped SnO_2 nanoparticles annealed at different temperatures. The spectra consist of six bands; the bands at 480, 640, and 780 cm^{-1} are attributed to the fundamental phonon modes E_g , A_{1g} , and B_{2g} of SnO_2 , respectively. On the other hand, the two weak bands appeared at 314, and 360 cm^{-1} and the intense band at 580 cm^{-1} (S1) are assigned to surface phonon modes (Zuo *et al.* 1994, Rumyantseva *et al.* 2005). The S1 band has been found in SnO_2 nanostructures with increasing intensity as the particle size is reduced (Diéguez *et al.* 2001). It is evident that the increase in annealing temperature leads to an improvement of crystallinity of the rutile SnO_2 nanostructures (intense A_{1g} Raman band).

For the Ag-doped SnO_2 nanoparticles, there appeared Raman peaks correspond to the E_g and A_{1g} vibrational modes, two surface modes at 250 and 340 cm^{-1} , and the S1 band at 580 cm^{-1} (Fig. 4). Ag doping generated a strong distortion of the crystalline structure which can affect the relative line-width and position of the Raman peaks (Yu *et al.* 1997). However, the Ag-doped

Table 1 Variation of crystallite size with annealing temperature for the SnO_2 and SnO_2 :Ag nanoparticles

Sample	Crystallite Size (nm)
SnO_2 (RT)	4.5
SnO_2 (300°C)	5.0
SnO_2 (700°C)	7.6
SnO_2 :Ag (1.0 %, RT)	6.0
SnO_2 :Ag (1.0 %, 700°C)	11.3
SnO_2 :Ag (5.0 %, RT)	5.0
SnO_2 :Ag (5.0 %, 700°C)	10.0

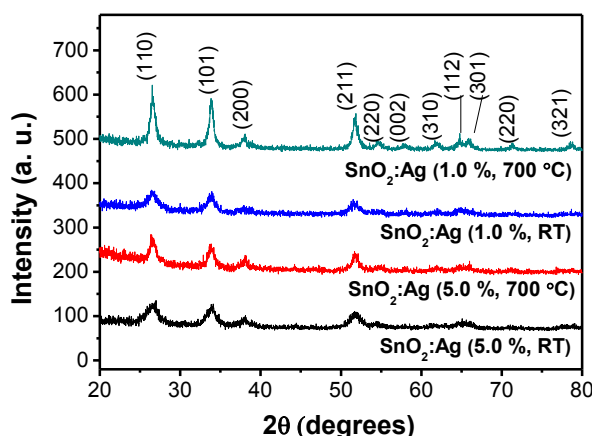


Fig. 2 X-ray diffraction patterns of the 1.0 and 5.0 % Ag-doped SnO_2 nanoparticles before and after thermal annealing at 700°C

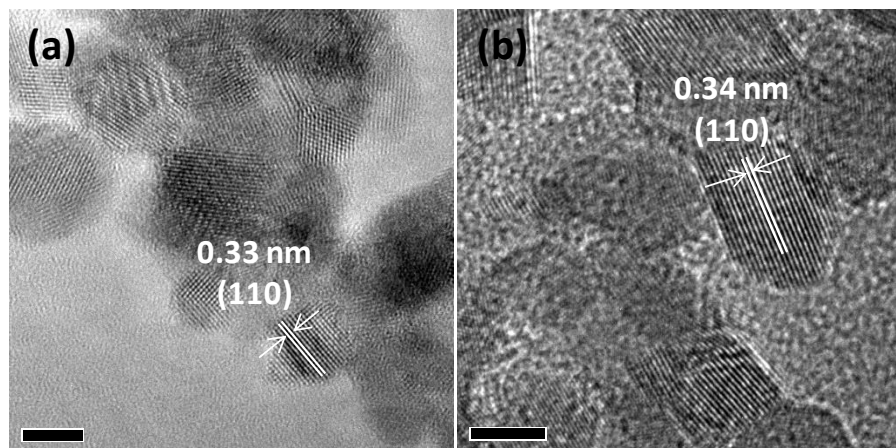


Fig. 3 Typical high resolutionTEM images of SnO₂ nanoparticles (a) before, and (b) after air annealing at 700°C. The interplaner spacing 0.33-0.34 nm correspond to the (110) planes of SnO₂ in tetragonal phase

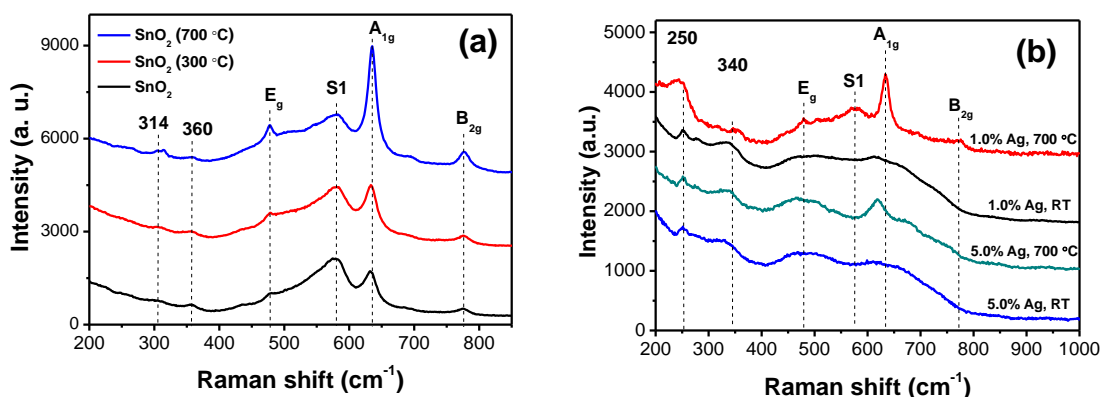


Fig. 4 Raman spectra of the (a) undoped, and (b) Ag-doped SnO₂ nanoparticles annealed at different temperatures

SnO₂ nanoparticles annealed at 700°C revealed intense and well defined Raman peaks suggesting their higher degree of crystallinity.

Fig. 5 presents the room temperature PL spectra of the undoped SnO₂ nanoparticles. All the spectra consist of a wide emission band spreading from 400 to 800 nm, with maxima at around 550 nm. This emission band has been associated essentially to the presence of point defects, such as oxygen vacancies (Luo *et al.* 2006) in SnO₂ nanoparticles. As can be seen, the unannealed SnO₂ sample exhibits highest PL intensity, which decreases with increasing annealing temperature. The decrease of emission intensity indicates a reduction of point defects in the SnO₂ particles on thermal annealing.

Fig. 6 depicts the TL glow curves of the undoped SnO₂ samples as a function of irradiation dose. As can be noticed, all the TL glow curves contain overlapping peak structures characteristic of polycrystalline nanophosphors with high concentration of surface atoms and defects at multiple

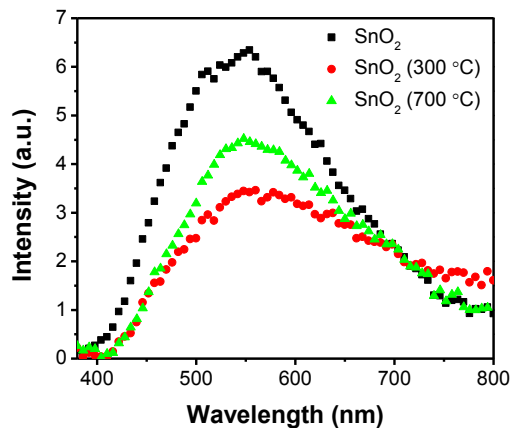


Fig. 5 Room temperature PL spectra of undoped SnO₂ nanoparticles annealed at different temperatures

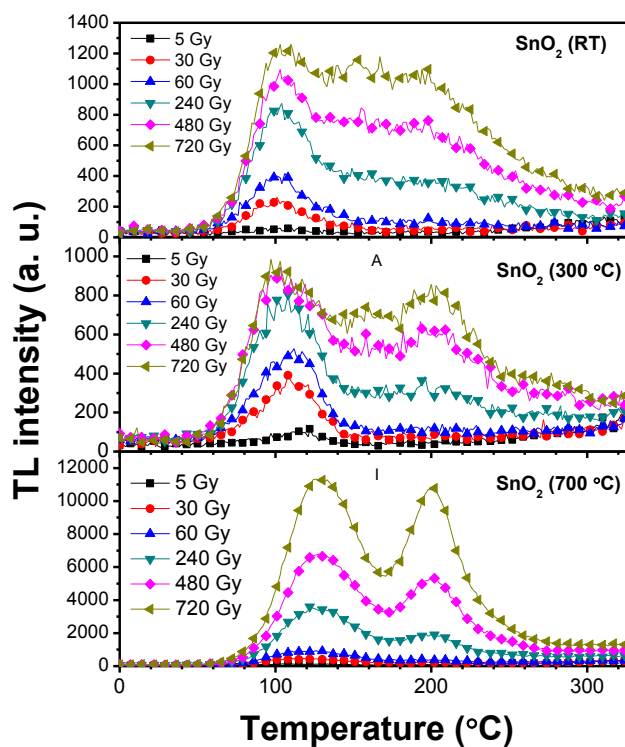


Fig. 6 TL glow curves of annealed and unannealed SnO₂ nanoparticles after exposing them with different radiation doses

nanograin boundaries (Reddy *et al.* 2011). It has been recognized that nanophosphors display wider TL peaks as compared to their bulk counterparts as well as lower TL intensity and high radiation resistance (Kortov *et al.* 2010, Salah *et al.* 2011). Significant increase of TL sensitivity

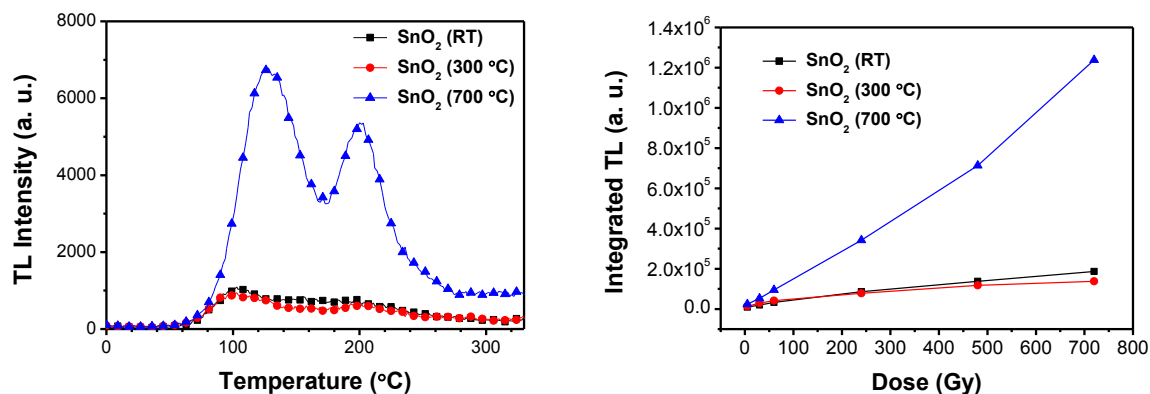


Fig. 7 (a) TL glow curves of SnO₂ nanoparticles annealed at different temperatures after exposing to 480 Gy beta radiation, and (b) variation of their Integrated TL intensity with radiation dose

for our 700 °C annealed SnO₂ nanoparticles (Fig. 6) evidences their enhanced radiation resistance behavior, which is a well known characteristic of nanophosphors.

Fig. 7 depicts the variation of integrated TL intensity of undoped SnO₂ nanoparticles annealed at different temperatures, as a function of irradiation dose. Both the as-grown and 300 °C air annealed samples produced linear and sub-linear dose behaviors for the lower (5 to 240 Gy) and high (240 to 720 Gy) radiation doses, respectively. A remarkable increase of TL sensitivity is observed for the sample annealed at 700 °C. However, the dose behavior of the samples is linear only for the lower doses. The dose behavior is super-linear in the intermediate and higher dose ranges.

As can be seen in Fig. 6, the most prominent TL peaks are located around 128 and 206 °C with a lesser intense peak around 150 °C. The same set of overlapped TL glow peaks with distinct intensity ratios appeared for the Ag-doped SnO₂ nanoparticles irrespective of their annealing temperature (Fig. 8). The TL sensitivity of the nanoparticles increases with the increase of annealing temperature. The TL sensitivity is highest for the 1.0% Ag doped SnO₂ nanoparticles after annealing them at 700 °C. The dose enhancing and dose linearity behaviors of the Ag-doped nanophosphors are clear from their integrated TL intensity variations with irradiation dose depicted in Fig. 9. It should be recalled that on thermal annealing at 700 °C, the crystallite size of the SnO₂:Ag (1.0%) sample increased from 6.0 (unannealed) to 11.3 nm (annealed at 700 °C) and most probably that is the main reason behind its strong TL sensitivity. On the other hand, incorporation of Ag in the SnO₂ nanoparticles in higher concentration causes an increase of microstrain in the form of some tensile stress along the *c* axis and compressive stress parallel to it (Sánchez-Zeferino *et al.* 2008). On increasing Ag-content, the microstrain in the nanoparticles increases. On the other hand, both Ag-incorporation and thermal annealing cause substantial increase of particle size. Both of these factors are responsible for the drastic changes observed in the TL characteristics observed in the Figs. 6, 7 and 9.

As has been stated earlier, the thermal treatment at 700 °C improves both the crystallinity and crystallite size of the SnO₂:Ag nanoparticles. The annealing also dramatically increases the TL sensitivity of the samples as displayed in Fig. 9. The picture is even clear in the Fig. 7(a), which illustrates TL glow-curves of the undoped SnO₂ sample after annealing at different temperatures, recorded after 480 Gy beta radiation exposures. For the as-grown and 300 °C annealed samples, the

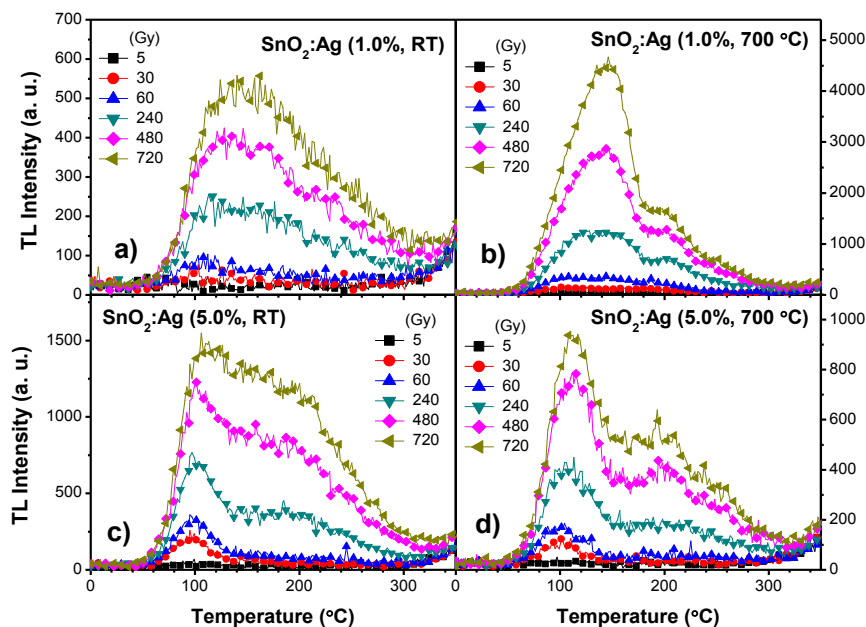


Fig. 8 TL glow curves of as-grown and 700°C annealed SnO₂:Ag nanoparticles after exposing them to radiations of different doses

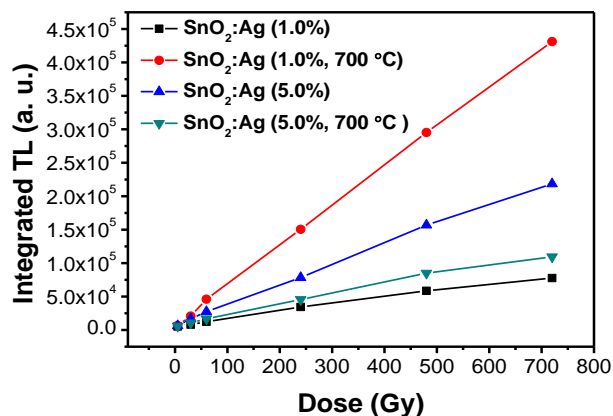


Fig. 9 Variation of integrated TL intensity of the Ag-doped SnO₂ nanoparticles with the dose of irradiation

TL glow-curves exhibit two peaks with maxima around 105 and 202°C. The thermal treatment at 300°C did not induce any significant change in the TL curves either in shape or in intensity. However, the TL curve of the sample annealed at 700°C revealed two prominent TL peaks with maxima at 126 and 206°C and intensities of about five times higher than the former samples. On the other hand, the TL glow-curves of the 1.0% Ag-doped SnO₂ nanoparticles revealed two predominant TL peaks centered around 143 and 202°C, which are overlapped for the unannealed sample (Figs. 8(a) and 8(c)). It is also evident that the TL intensity of the annealed sample is

substantially higher than that of the unannealed sample. However, though the intensity of the TL peaks increased about 2 folds for the 5.0% Ag-doped sample, a thermal treatment at 700°C reduces its TL response. A segregation of Ag ions/atoms on the surface of the SnO₂ nanoparticles or the formation of Ag clusters at the interstitial lattice sites might be responsible for the observed decrease of TL response of the samples, as the metallic clusters act as non-radiative recombination centers for the thermally activated charge carriers.

The Ag-doped SnO₂ particles revealed quite distinct dose behaviors in comparison with the undoped nanoparticles (Figs. 7 and 9), especially for the higher-dose range. While the integrated TL intensity of all the Ag-doped nanophosphors varied linearly with the irradiation dose up to 500 Gy, the TL response is substantially higher for the 1.0% Ag-doped sample after annealing at 700°C. The superior TL response and dose linearity of the sample are associated to its Ag-doping at low concentration and thermal annealing. The annealing process stabilizes the trapping/detrapping levels and recombination characteristics of the lightly Ag-doped SnO₂ nanoparticles, perhaps by homogenizing their strain-induced lattice defects. While the same phenomena can occur in the 5.0% Ag-doped SnO₂ nanoparticles, their ultimate TL responses are substantially lower due to the formation of Ag clusters either at the interstitial sites or at the surface. Of course a more detailed investigation is required to account for these nanometric TL effects with certainties. What is clear from the results of this investigation is a suitable thermal annealing process (annealing at 700°C for SnO₂) and adequate doping can produce highly efficient thermoluminescent nanophosphors suitable for dosimetric applications at higher radiation doses.

4. Conclusions

In summary, both Ag-doping and post-growth thermal annealing drastically modify the luminescence behaviors of SnO₂ nanoparticles. The high temperature air-annealing process improves the crystallinity of SnO₂ nanoparticles, enhancing their average grain-size and reducing lattice-strains. While Ag-doping at a lower concentration localizes Ag atoms at the interstitial sites of the SnO₂ lattice, a high concentration of incorporated Ag and subsequent thermal annealing generates Ag clusters at the interstitial sites or at the surface of the nanoparticles. Formed Ag clusters inside or at the surface of SnO₂ nanoparticles act as non-radiative recombination centers, causing a reduction of their TL sensitivity. Our results indicate that the SnO₂ nanoparticles with a limited amount of Ag content and annealed at 700°C have a higher TL sensitivity as well as dose linearity at higher doses, properties which are suitable for dosimetry and controlled radiation therapy applications.

Acknowledgements

The authors are thankful to CONACyT, Mexico and VIEP-BUAP for financial helps extended through the project grants # CB-2010/151767 and VIEP/EXC/2013, respectively.

References

Baik, N.S., Sakai, G., Shimano, K., Miura, N. and Yamazoe, N. (2000), "Hydrothermal treatment of tin oxide sol solution for preparation of thin-film sensor with enhanced thermal stability and gas sensitivity",

- Sens. Actuators B*, **65** (1-3), 97-100.
- Chen, H.T., Wu, X.L., Zhang, Y.Y., Zhu, J., Cheng, Y.C. and Chu, P.K. (2009), "A novel hydrothermal route to synthesize solid SnO₂ nanospheres and their photoluminescence property", *Appl. Phys. A*, **97** (3), 581-585.
- Diéguez, A., Rodriguez, A.R., Vilá, A. and Morante, J.R. (2001), "The complete Raman spectrum of nanometric SnO₂ particles", *J. Appl. Phys.*, **90**(3), 1550-1557.
- Epifani, M., Arbio, J., Pellicer, E., Comini, E., Siciliano, P., Faglia, G. and Morante, J.R. (2008), "Synthesis and gas-sensing properties of Pd-doped SnO₂ nanocrystals. A case study of a general methodology for poping metal oxide nanocrystals", *Cryst. Growth Des.*, **8**(5), 1774-1778.
- German, R.M. (1996), *Sintering theory and practice*, John Willey & Sons, New York.
- Gnanam, S. and Rajendran, V. (2010), "Synthesis of tin oxide nanoparticles by sol-gel process: effect of solvents on the optical properties", *J. Sol-Gel Sci. Technol.*, **53**(3), 555-559.
- Kortov, S.V. (2010), "Nanophosphors and outlooks for their use in ionizing radiation detection", *Rad. Meas.*, **45** (3), 512-515.
- Lee, E.J.H., Ribeiro, C., Giraldi, T.R., Longo, E. and Leite, E.R. (2004), "Photoluminescence in quantum-confined SnO₂ nanocrystals: Evidence of free exciton decay", *Appl. Phys. Lett.*, **84**(10), 1745-1747.
- Lee, J.I., Chang, I., Kim, J.L., Kim, B.H., Kim, S.I., Chung, K.S. and Choe, H.S. (2011), "LiF: Mg, Cu, Si material with intense high-temperature TL peak prepared by various thermal treatment conditions", *Rad. Meas.*, **46**(12), 1496-1499.
- Luo, S., Fan, J., Liu, W., Zhang, M., Song, Z., Lin, C., Wu, X. and Chu, P.K. (2006), "Synthesis and low-temperature photoluminescence properties of SnO₂ nanowires and nanobelts", *Nanotechnology*, **17**(6), 1695-1699.
- Pal, U., Pal, M. and Sánchez Zeferino R. (2012), "Gram-scale synthesis of highly crystalline, 0-D and 1-D SnO₂ nanoclusters through surfactant-free hydrothermal process", *J. Nanopart. Res.*, **14**(7), 969-10.
- Qia, Q., Zhanga, T., Liua, L. and Zheng, X. (2009), "Synthesis and toluene sensing properties of SnO₂ nanofibers", *Sens. Actuators B*, **137**(2), 471-475.
- Qian, L.H., Wanga, K., Fang, H.T., Lia, Y. and Maa, X.L. (2007), "Au nanoparticles enhance CO oxidation onto SnO₂ nanobelt", *Mater. Chem. Phys.*, **103**(1), 132-136.
- Reddy, A.J., Kokila, M.K., Nagabhushana, H., Rao, J.L., Shivakumara, C., Nagabhushana, B.M., Chakradhar, R.P. (2011), "EPR, thermo and photoluminescence properties of ZnO nanopowders", *Spectrochim. Acta A Mol. Biomol. Spectrosc.*, **81**(1), 59-63.
- Rumyantseva, M.N., Gaskov, A.M., Rosman, N., Pagnier, T. and Morante, J.R. (2005), "Raman surface vibration modes in nanocrystalline SnO₂ prepared by wet chemical methods: correlations with the gas sensors performances", *Chem. Mater.*, **17**(4), 893-901.
- Salah, N. (2011), "Nanocrystalline materials for the dosimetry of heavy charged particles: A review", *Radiat. Phys. Chem.*, **80**(1), 1-10.
- Sánchez-Zeferino, R., Pal, U., Barboza-Flores, M., Santiago, P., Rendón, L. and Garibay Febles, V. (2012), "Hydrothermally grow ultra-fine SnO₂ and SnO₂: Ag nanoparticles and their optical characteristics", *Sci. Adv. Mater.*, **4**(5/6), 591-596.
- Yang, H.Y., Yu, S.F., Liang, H.K., Lau, S.P., Pramana, S.S., Ferraris, C., Cheng, C.W. and Fan, H.J. (2010), "Ultraviolet electroluminescence from randomly assembled n-SnO₂ nanowires-p-GaN:Mg heterojunction", *Appl. Mater. Interfaces*, **2**(4), 1191-1194.
- Yu, K.N., Xiong, Y., Liu, Y. and Xiong, C. (1997), "Microstructural change of nano-SnO₂ grain assemblages with the annealing temperature", *Phys. Rev. B*, **55**(4), 2666-2671.
- Zuo, J., Xu, C., Liu, X., Wang, C., Wang, C., Hu, Y. and Qian, Y. (1994), "Study of the Raman spectrum of nanometer SnO₂", *J. Appl. Phys.*, **75**(3), 1835-1836.